Development/Plasticity/Repair

Secreted Frizzled Related Proteins Modulate Pathfinding and Fasciculation of Mouse Retina Ganglion Cell Axons by Direct and Indirect Mechanisms

Séverine Marcos,[1,2,3] **Francisco Nieto-Lopez,**[1,2,3] **Africa Sandonìs,**[1,2,3] **Marcos Julian Cardozo,**[1,2,3] **Fabiana Di Marco,**[1] **Pilar Esteve,**[1,2,3] **and Paola Bovolenta**[1,2,3]

[1]Centro de Biología Molecular Severo Ochoa, Consejo Superior de Investigaciones Científicas–Universidad Autónoma de Madrid, Madrid 28049, Spain, [2]Centro de Investigación Biomédica en Red de Enfermedades Raras, Madrid 28049, Spain, and [3]Instituto Cajal, Consejo Superior de Investigaciones Científicas, 28002 Madrid, Spain

Retina ganglion cell (RGC) axons grow along a stereotyped pathway undergoing coordinated rounds of fasciculation and defasciculation, which are critical to establishing proper eye–brain connections. How this coordination is achieved is poorly understood, but shedding of guidance cues by metalloproteinases is emerging as a relevant mechanism. Secreted Frizzled Related Proteins (Sfrps) are multifunctional proteins, which, among others, reorient RGC growth cones by regulating intracellular second messengers, and interact with Tolloid and ADAM metalloproteinases, thereby repressing their activity. Here, we show that the combination of these two functions well explain the axon guidance phenotype observed in *Sfrp1* and *Sfrp2* single and compound mouse mutant embryos, in which RGC axons make subtle but significant mistakes during their intraretinal growth and inappropriately defasciculate along their pathway. The distribution of *Sfrp1* and *Sfrp2* in the eye is consistent with the idea that Sfrp1/2 normally constrain axon growth into the fiber layer and the optic disc. Disheveled axon growth instead seems linked to Sfrp-mediated modulation of metalloproteinase activity. Indeed, retinal explants from embryos with different *Sfrp*-null alleles or explants overexpressing ADAM10 extend axons with a disheveled appearance, which is reverted by the addition of Sfrp1 or an ADAM10-specific inhibitor. This mode of growth is associated with an abnormal proteolytic processing of L1 and *N*-cadherin, two ADAM10 substrates previously implicated in axon guidance. We thus propose that Sfrps contribute to coordinate visual axon growth with a dual mechanism: by directly signaling at the growth cone and by regulating the processing of other relevant cues.

Key words: axon guidance; metalloproteinase; optic chiasm; optic disc; Sfrp; visual pathway

Introduction

In vertebrates, retina ganglion cell (RGC) axons convey visual information from the eye to the brain through a long pathway that is stereotypically composed of different segments. The fiber layer and the optic nerve and tract are segments in which axons grow tightly fasciculated to their neighbors. Axon initiation, navigation through the optic disc (OD) and chiasm, or the selection of the target neuron within the lateral geniculate nucleus or superior colliculus represent instead "decision" steps in which axons can take different routes, diverging if necessary from the

behavior of their neighbors. Linear segments and choice points alternate along the pathway (Bovolenta and Mason, 1987). Therefore, coordination among extrinsic cues that mediates selective axon fasciculation/defasciculation and those that provide steering information to growth cones is critical for proper development of the visual system.

Functional studies in vertebrates have shown that members of evolutionary conserved families of attractive and repulsive guidance cues, such as Slits, Semaphorins, or Ephrins, and morphogenetic signaling pathways activated by Shh or Wnts are among the extrinsic cues that direct RGC growth cones navigation at choice points (Bao, 2008; Petros et al., 2008; Sánchez-Camacho and Bovolenta, 2009; Erskine and Herrera, 2014). Cell adhesion molecules, integrins, or cadherins instead mostly mediate RGC axon fasciculation (Bao, 2008).

What coordinates the activity of these extrinsic cues is still poorly understood, although members of the matrix metalloproteinase and A Disintegrin And Metalloproteinase (ADAM) families are emerging as attractive candidates (McFarlane, 2003; Bai and Pfaff, 2011). Indeed, ADAM10 or its *Drosophila* homolog *kuzbanian* terminates high-affinity interaction between Ephrins and their Eph receptors (Hattori et al., 2000) and cleaves the extracellular domain of Robo (Coleman et al., 2010) and Neuro-

pilin1 receptors (Romi et al., 2014), thereby changing the sensitivity of growth cones to Slit and Sema3A ligands, respectively. Furthermore, ADAM10 sheds the extracellular domain of N-cadherin and L1 (Reiss et al., 2005; Riedle et al., 2009; Malinverno et al., 2010), which both participate in selective fasciculation of visual axons (Riehl et al., 1996; Mi et al., 1998; Lyckman et al., 2000; Masai et al., 2003). Therefore, spatiotemporally regulated ADAM activities might plausibly coordinate visual projection development, as also supported by metalloproteinase inhibitory studies in Xenopus (Webber et al., 2002).

Sfrps are bimodular, highly diffusible factors, which, in addition to acting as negative and positive modulators of Wnt signaling (Bovolenta et al., 2008; Mii and Taira, 2009; Esteve et al., 2011a), interact with metalloproteinase of the Tolloid and ADAM families, thereby controlling the processing of their respective substrates (Lee et al., 2006; Muraoka et al., 2006; Kobayashi et al., 2009; Esteve et al., 2011b). Sfrp1 and Sfrp2 are strongly expressed during vertebrate eye development (Terry et al., 2000; Liu et al., 2003a; Blackshaw et al., 2004). In mice, Sfrp1 and Sfrp2 are redundantly required to specify the periphery of the retina by promoting canonical Wnt signaling activation (Esteve et al., 2011a) and to control retinal neurogenesis by inhibiting ADAM10 activity (Esteve et al., 2011b). Furthermore, chick and mouse RGC axons respond to Sfrp1 (Rodríguez et al., 2005; Sebastián-Serrano et al., 2012) and exposure of Xenopus RGC growth cones to a focalized source of the protein reorients their growth with a mechanism that involves the expression of the Frizzled 2 receptor (Rodríguez et al., 2005).

Here, we show that, in the absence of Sfrp1 and Sfrp2, RGC axons are less tightly packed and make subtle but significant mistakes as they grow along their pathway. These defects are explained by the multifunctional role of Sfrp proteins in the regulation of cell–cell communication, which involves both direct signaling at the growth cone and the control of proteolytical processing of other relevant guidance cues.

Materials and Methods

Animals. Sfrp1$^{-/-}$;Sfrp2$^{+/-}$ mice were generated and intercrossed or backcrossed to C57BL/6J to obtain the different single or double Sfrp1$^{-/-}$ and Sfrp2$^{-/-}$ and control wild-type (wt) mice (Satoh et al., 2006; Esteve et al., 2011b). Embryos of either sex were obtained from timed mating of the resulting strains. The date of the vaginal plug was considered as embryonic day 0.5 (E0.5). Compound mutant embryos do not survive beyond E16–E16.5, limiting their analysis (Satoh et al., 2006; Esteve et al., 2011b). Animals were used according to institutional and national guidelines.

In situ hybridization. For in situ hybridization (ISH), E14.5 embryos were fixed by immersion in 4% PFA in phosphate buffer 0.1 M, pH 7.2, for 3 h. Older embryos were transcardiacally perfused with the same fixative and postfixed for 2 h. Tissue was washed in PBS, cryoprotected overnight in 30% sucrose/PBS solution, embedded, and frozen in 7.5:15% gelatin/sucrose solution and serial sectioned in the frontal plane using a cryostat (Leica). ISH was performed as described previously (Marcos et al., 2009) with the following specific probes: Sfrp1, Sfrp2, Shh, Netrin1, EphB2, Adam10 and the heterologous rat Slit1, Slit2, and Robo2.

Immunostaining. Cryosections were permeabilized with PBS containing 0.1% Triton X-100 (PBT) and immunostained in PBT containing 1% normal goat serum with the following primary antibodies: rabbit anti-Sfrp1 (1:500; Abcam), rat anti-Sfrp2 (a kind gift from S. Hauck; (Hauck et al., 2012), mouse anti-βIII-tubulin (TuJ1; 1:1000; Promega), rabbit anti-neurofilament M (1:500; Millipore), goat anti-Robo2 (1:500, a kind gift from Prof. F. Murakami (Tamada et al., 2008); rabbit anti-L1-CAM (1:500; (Lemmon et al., 1989); mouse anti-N-cadherin (1:500; Invitrogen). Primary antibodies were detected with Alexa Fluor 488, Alexa Fluor 568 (Invitrogen), or biotin-conjugated (Jackson Laboratory) specific sec-

ondary antibodies (1:1000). Biotin IgGs were visualized using streptavidin-POD followed by DAB incubation. For immunofluorescence, sections were counterstained with DAPI (1 μg/ml; Vector Laboratories). Sfrp2 immunosignal in Figure 1, I–L′, was amplified with tyramide (PerkinElmer).

DiI and DiO tracing. The path of RGC axons was visualized using a 0.4% solution of 1,1′-dioctadecyl-3,3,3′,3′-tetramethylindocarbocyanine (DiI, D282) or 3,3′-dioctadecyloxacarbo-cyanine perchlorate (DiO, D275; Invitrogen) dissolved in 4:10% dimethylformamide/sucrose solution. For intraretinal tracings, E15.5 retinas were dissected out, fixed with 4% PFA, and a tiny amount of DiI or DiO solution was injected in the dorsal or ventral periphery. Tissue was thereafter incubated for 1 h at 37°C. For unilateral anterograde tracings, the lens was removed from E15.5 heads to expose the OD, into which a small DiI crystal was inserted. Heads were stored in the dark for 2 weeks at 37°C. Brains were then dissected, the telencephalic vesicles were removed, and the exposed optic chiasm and tract were analyzed. For unilateral retrograde tracings, E15.5 heads were fixed as above, brains were carefully freed from the ventral skull, and small DiI crystals were placed in the initial segment of the optic tract. Heads were stored in the dark for 2 weeks at 37°C. Thereafter, both eyes were isolated, embedded in 4% agarose, and sectioned at 50 μm thickness with a vibratome (Leica).

Retinal explants. Explants from E15.5 wt or Sfrp2$^{-/-}$ and Sfrp1$^{-/-}$; Sfrp2$^{-/-}$ central retinas were grown on glass coverslips coated with poly-D-lysine (10 μg/ml; Sigma) and laminin (10 μg/ml; Invitrogen) in DMEM/F12/N2 (Invitrogen) at 37°C as described previously (Sánchez-Camacho and Bovolenta, 2008). Explants were grown in the presence or absence of purified Sfrp1 (500 ng/ml; Sigma; Esteve et al., 2003), the ADAM10-specific inhibitor GI254023X resuspended in DMSO (5 μM; a gift from Dr. A. Ludwig; Ludwig et al., 2005), or DMSO alone. After 48 h, explants were fixed in 2% PFA containing 11% sucrose at 37°C and stained with anti-βIII-tubulin antibodies. To determine the effect of ADAM10 on retinal axon fasciculation in vitro, E13.5 embryos (at least 10 for each condition) were electoporated ex utero with pRK5M-Adam10 (catalog #31717; Addgene) mixed with pCAG-GFP (5:1) or pCAG-GFP alone. Soon after, retinas were isolated and incubated in DMEM/F12/N2 (Invitrogen) overnight. The targeted GFP-positive regions of the retinas were dissected and grown as explants as described above. After 48 h, explants were fixed and immunostained with antibodies against GFP and anti-βIII-tubulin.

Western blots. E16.5 retinas, together with the optic nerves and tracts from wt, Sfrp1$^{-/-}$, Sfrp2$^{-/-}$, and Sfrp1$^{-/-}$;Sfrp2$^{-/-}$ embryos, were isolated and homogenized in lysis buffer (150 mM NaCl, 2% Triton X-100, 50 mM Tris, pH 8) supplemented with a proteinase inhibitor mixture (Roche) and PMSF. In other experiments, retinal explants electroporated as described above were washed from the culture medium and directly incubated in a modified lysis buffer (150 mM NaCl, 2% Triton X-100, 50 mM Tris, pH 8, 10 mM CaCl$_2$) supplemented with a mixture of proteinase inhibitors (Roche) and PMSF. In all cases, protein content was quantified and tissue extracts (50 μg) were separated by electrophoresis on SDS polyacrylamide gels and transferred onto PVDF membranes. After blocking in TBS/0.1% Tween/5% nonfat milk, the membranes were incubated overnight at 4°C with rabbit polyclonal 74-5H7 that recognizes the L1 cytoplasmic portion (a kind gift from Dr. V. Lemmon; Lemmon et al., 1989) or mouse mAb against the C-terminal domain of N-cadherin (1:500; Invitrogen) and mouse anti-α-tubulin (1:10.000; Sigma) used as a loading control. Membranes were then incubated with peroxidase-conjugated secondary antibodies followed by ECL Advanced Western Blotting Detection Kit (GE Healthcare). The immunoreactive bands were quantified by densitometry and the amount of proteolyzed fragment was calculated as the ratio of fragment/native/α-tubulin band values. Western blots were repeated at least three times, obtaining very similar results. To determine the specificity of α-Sfrp2 antibody, eyes from E14.5 wt and Sfrp2$^{-/-}$ embryos were processed as above. Lysates were incubated with heparin-acrylic beads (Sigma) for 1 h and beads were recovered by centrifugation. Heparin-binding proteins were resolved on SDS polyacrylamide gels, transferred, and the PDVF membrane incubated with an anti-Sfrp2 antibody. The membrane was processed as above.

Image and statistical analysis. Tissue was analyzed with M205FA stereomicroscope or a DM CTR5000 microscope equipped for fluorescence microscopy and photographed with a DFC500 camera (Leica Microsystems). Confocal analysis was performed with LSM510 META equipment (Zeiss). Quantitative analysis was performed using ImageJ software. At least 10 explants per condition were analyzed to quantify axon fasciculation. Three images per explant were acquired. A line was drawn perpendicular to the axis of main neurite outgrowth and gray values along this line were recorded. The width of axon fascicles was calculated as the number of consecutive points with gray values >25 present along the established line (values <25 were considered background). Student's t test and Bonferroni's test were used to compare mean values of fascicle width calculated for the different conditions. Differences between calculated averages were considered significant when $p < 0.05$. The degree of axon fasciculation was also determined as the percentage of fascicles with width greater than or equal to the given pixels as indicated in the figures. In ADAM10-overexpression experiments, the degree of axon fasciculation was evaluated as the percentage of green fascicles, with the procedure described above.

Results

Sfrp1 and Sfrp2 are expressed in the eye and distributed along the mouse visual pathway

Previous studies showed that *Sfrp1* and *Sfrp2* are expressed during eye development. In chick and medaka fish, *Sfrp1* mRNA localizes to the retinal neuroepithelium, the OD, chiasm, and the initial portion of the optic tract (Terry et al., 2000; Esteve et al., 2003; Esteve et al., 2004; Rodríguez et al., 2005). In mice instead, *Sfrp1* mRNA was detected in the retinal pigment epithelium, the ciliary margin (Liu et al., 2003a; Esteve et al., 2011b), and the RGC layer (Fig. 1A), but not in the chiasm or the optic tract region (Fig. 1C and data not shown). Consistent with the expression in RGC, Sfrp1 protein localized to the growing RGC axons both *in vivo* and in dissociated cultures (Fig. 1B,D,E). *Sfrp2*, which mostly localizes to the RGC layer in the chick retina (Lin et al., 2007), was instead strongly expressed in the undifferentiated retinal neuroepithelium and in the proximal portion of the developing optic stalk (Fig. 1F). With development, Sfrp2 expression progressively became downregulated in the central retina forming a central[low] to peripheral[high] gradient in the dorsal retina, but maintained an even distribution in the ventral retina and in the glial cells that form the OD (Morcillo et al., 2006) (Fig. 1G). *Sfrp2* mRNA was still clearly detected in the retinal neuroepithelium at E16.5 with levels that became progressively lower up to birth (data not shown), also as described previously (Blackshaw et al., 2004; Trimarchi et al., 2008). Immunostaining with an antibody that specifically recognized the Sfrp2 protein (Hauck et al., 2012), as confirmed by the lack of specific signal in *Sfrp2*^{−/−} embryos in both immunostaining and Western blot analysis (Fig. 1L,L',J,M), demonstrated that Sfrp2 protein, in addition to that in the retinal progenitors (Fig. 1H,I,K), specifically localizes to nascent RGCs and in their axons at E13.5 (Fig. 1H), as well as in cells of the distal optic nerve (Fig. 1K'). Sfrp2 was not expressed in the ciliary margins (Fig. 1F,G,I; Liu et al., 2003a; Esteve et al., 2011b) or the diencephalon (data not shown).

Together, these data indicate that there are species-specific differences in the expression of *Sfrp1* and *Sfrp2* in the developing visual pathway. In mouse embryos, their pattern of distribution suggests a potential role in establishing a proper RGC axon trajectory.

Sfrp2 and Sfrp1 are required for correct intraretinal RGC pathfinding

We investigated whether genetic inactivation of *Sfrp1* and *Sfrp2* has functional consequences in RGC axon growth. Because *Sfrp2*
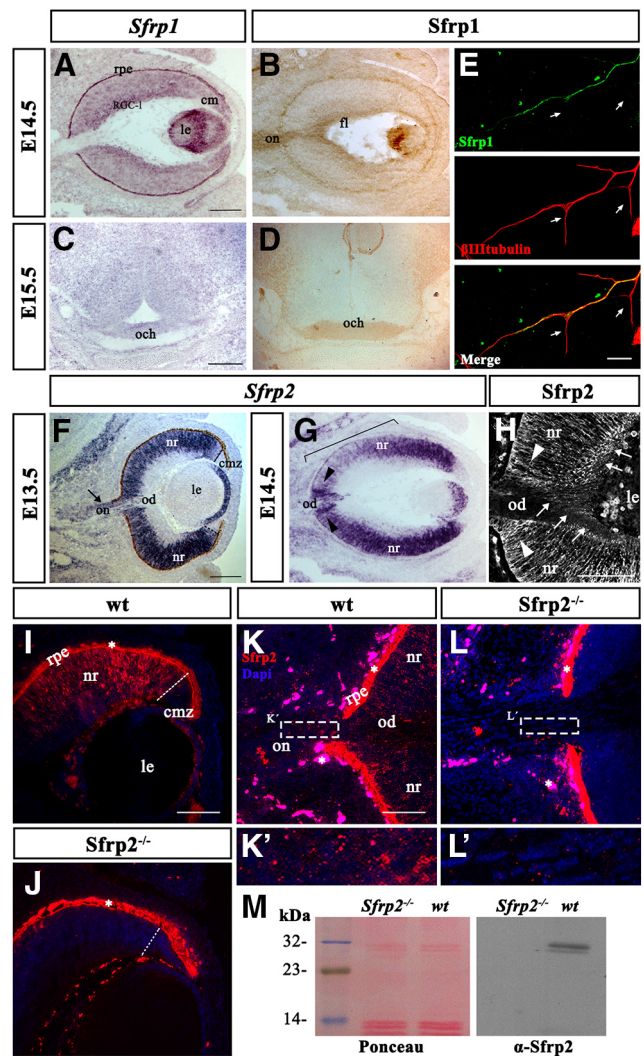

Figure 1. Expression of *Sfrp1* and *Sfrp2* in the proximal visual pathway. Transverse sections of E14.5 (**A**, **B**, **G**) and E13.5 (**F**, **H**, **I–L'**) retinas and E15.5 diencephalon (**C**, **D**) from wild-type (**A–D**, **F–K'**) and *Sfrp2*^{−/−} (**J**, **L**, **L'**) embryos hybridized with probes for *Sfrp1* (**A**, **C**) and *Sfrp2* (**F**, **G**) or immunostained with α-Sfrp1 (**B**, **D**) or α-Sfrp2 antibodies (**H–L'**). **E**, Dissociated culture from wt E14.5 retinas coimmunostained with α-Sfrp1 (green) and α-βIII-tubulin (red) antibodies. Note the expression of *Sfrp1* in the RGC layer (RGC-l), retina pigmented epithelium (rpe), ciliary margins (cm), and lens (le). Note also that *Sfrp1* mRNA is not present in the optic chiasm (och). Sfrp1 protein is abundantly detected in the RGC axons as they extend along the fiber layer (fl), optic nerve (on), and chiasm (**B**, **D**). This localization is confirmed in cultured neurons, where Sfrp1 localizes to the main neurite but it is absent from collateral branches (**E**, arrows). *Sfrp2* mRNA localizes instead to the proliferating neural retina (nr), and the initial portion of the developing optic nerve (on, arrow in **F**) and the glial cells of the OD (od; arrowheads in **G**) and lens, but it is absent from differentiated RGCs and the ciliary margins (cmz). At E14.5, *Sfrp2* expression in the dorsal-central retina begins to be downregulated (bracket in **G**). As demonstrated by the lack of any specific signal in *Sfrp2* mutant embryos (**J**, **L**, **L'**), Sfrp2 protein was specifically detected not only in the retinal progenitors but also in the nascent retinal ganglion cells (rgc) and their axons (**H**, arrows) as well as in cells of the optic nerve (**K'**). Asterisks in **I–L** indicate autofluorescent signal from the retina pigmented epithelium (rpe) and the red blood cells. **M**, Western blot analysis of Sfrp2 expression in heparin purified extracts of eyes from E14 wt and Sfrp2^{−/−} embryos. Note the presence of a specific band in wt but not mutant retinas (right). Each lane contains an equal amount of proteins as defined by Ponceau staining (left). Scale bars: 250 μm (**F**, **G**); 200 μm (**A–D**); 100 μm (**I–L**); 20 μm (**K'**, **L'**).

and *Sfrp1* are both expressed in the eye cup, we first searched for possible intraretinal pathfinding defects in single and compound mutant embryos.

Once generated, RGCs extend an axon that enters the fiber layer and grows with a radial orientation toward the OD posi-

tioned in the center of the retina. Therefore, axons of early-born RGCs, generated around the OD, have a short intraretinal growth, whereas those of late-born peripheral RGCs travel a longer distance before reaching the OD (Bao, 2008). To visualize this intraretinal trajectory, coronal sections and flat mounts from E15.5 wt and mutant retinas were immunostained with antibodies against neurofilament M that mostly label RGC axons at this stage (Fig. 2A–I). In wt and $Sfrp1^{-/-}$ retinas, axons were normally oriented toward the fiber layer, forming small, radially arranged bundles that never invaded the deeper layers of the retina (Fig. 2A,D,G and data not shown). In contrast, in $Sfrp2^{-/-}$ and $Sfrp1^{-/-};Sfrp2^{-/-}$ mutants, a significant amount of RGCs, mostly located at the periphery, aberrantly extended their axon toward the ventricular surface of the retina (Fig. 2B,C,J). Confocal analysis of the outer layers in flat-mounted preparations confirmed the presence of a significant amount of small ectopic axon bundles (Fig. 2H,I,K), a phenotype also observed upon inactivation of Robo-Slit signaling (Thompson et al., 2006b; Thompson et al., 2009). Ectopic fibers were most abundant in the ventral peripheral retina but nearly absent from the OD region (Fig. 2K). The frequency of these defects was consistent in all compound mutants analyzed, in agreement with the proposed $Sfrp1/Sfrp2$ functional redundancy (Satoh et al., 2006; Esteve et al., 2011b), but rather variable in $Sfrp2^{-/-}$ embryos, in which the number of ectopic axon bundles spanned from 5 to 60 per retina. In addition to these defects, in $Sfrp1^{-/-};Sfrp2^{-/-}$ retinas, a fraction of axons turned away from the OD, taking routes perpendicular to the main plane of growth (Fig. 2F). Despite these abnormal trajectories, at least part of the misrouted axons eventually left the eye because insertion of DiI crystals in the optic tract retrogradely labeled misprojecting RGCs in the periphery of the retina (Fig. 2L–N).

To define more precisely intraretinal axonal misprojections and to estimate their frequency, the trajectory of discrete axon bundles was visualized by the insertion of tiny crystals of DiI and DiO into the dorsal and ventral retinal periphery, respectively (Fig. 3A). This approach confirmed that in wt and $Sfrp1^{-/-}$ embryos RGC axons grew straight to the OD with occasional wiggling around its entry point (Fig. 3B,C,H) but ~50% of the traced $Sfrp1^{-/-};Sfrp2^{-/-}$ retinas contained axons that either individually or in small
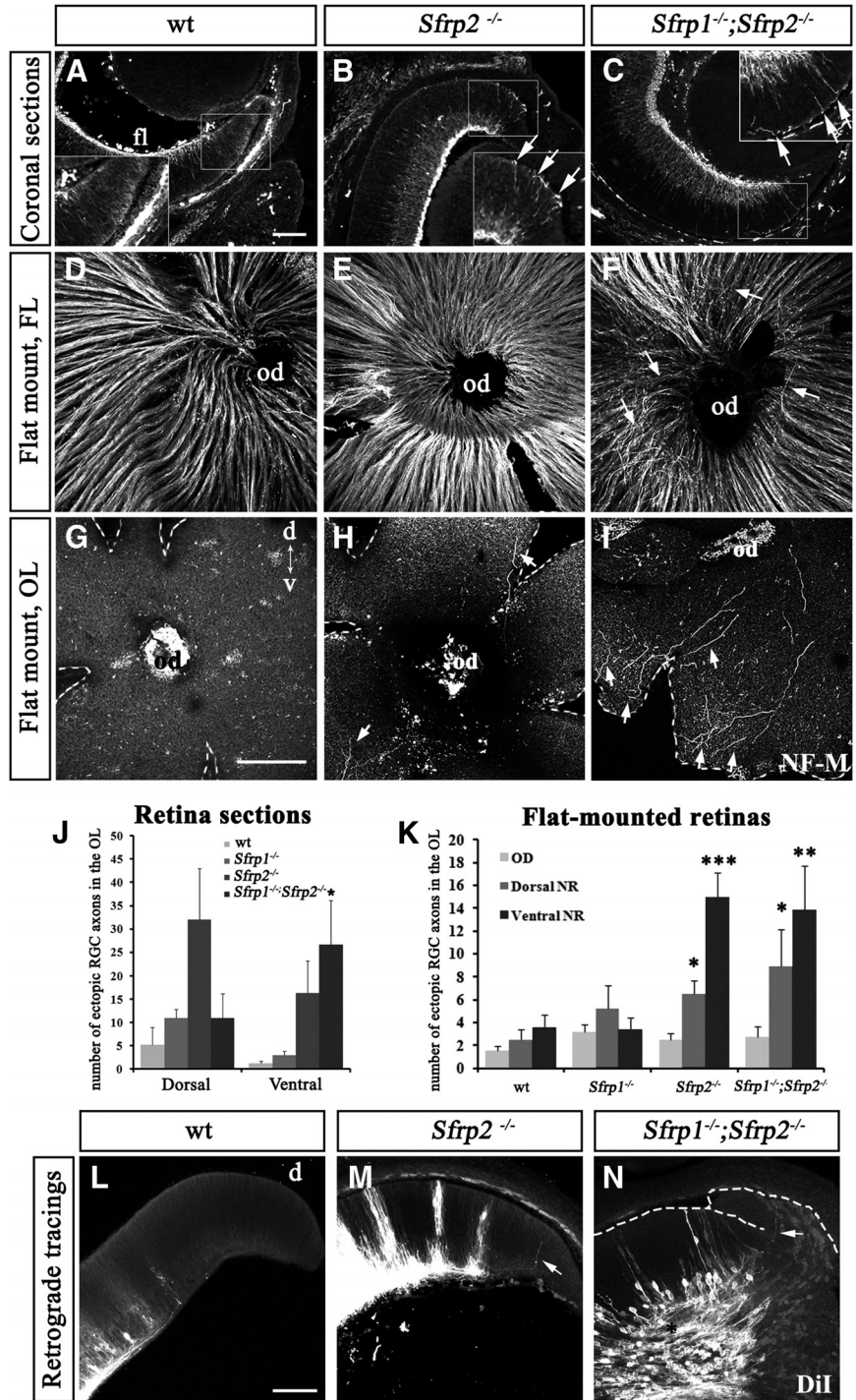

Figure 2. $Sfrp1/2$ are required for correct intraretinal organization of RGC axons. Coronal sections (**A–C**) and flat mounts (**D–I**) of retinas from E15.5 wt, $Sfrp2^{-/-}$, and $Sfrp1^{-/-};Sfrp2^{-/-}$ embryos immunostained with α-NF-M antibodies. Images in **D–I** are confocal planes of the fiber (**D–F**) and outer (**G–I**) layers of the retinas. Note that, in wt, all RGC axons extend toward the fiber layer (fl, in **A**), whereas in the mutants, several axons from peripheral RGCs invade the outer retina (arrows in insets in **B**, **C**). Image in **B** shows the dorsal retina; images in **A** and **C**, the ventral retina. Axons invading the outer retina are also observed in flat-mount preparations (**H**, **I**). Note also that, in compound mutants, RGC axon bundles in the fiber layer are less defined and often present axons abnormally extending away from the OD (od, arrowheads in **F**). **J**, Mean ± SEM number of ectopic axons per coronal section in the dorsal or ventral periphery of wt ($n = 6$), $Sfrp1^{-/-}$ ($n = 10$), $Sfrp2^{-/-}$ ($n = 6$), and $Sfrp1^{-/-};Sfrp2^{-/-}$ ($n = 6$) deficient retinas. *$p < 0.05$ compared with wt. **K**, Mean ± SEM number of axons or small axon bundles located in the OD region, in the dorsal or ventral outer retina in wt ($n = 12$), $Sfrp1^{-/-}$ ($n = 19$), $Sfrp2^{-/-}$ ($n = 14$), and $Sfrp1^{-/-};Sfrp2^{-/-}$ ($n = 8$) flat-mounted retinal preparations. *$p < 0.05$; **$p < 0.01$; ***$p < 0.001$ compared with wt; Student's t test. **L–N**, Coronal sections of wt (**L**), $Sfrp2^{-/-}$ (**M**), and $Sfrp1^{-/-};Sfrp2^{-/-}$ (**N**) E15.5 retinas after DiI retrograde tracings from the optic tract. Note that, in $Sfrp2^{-/-}$ and $Sfrp1^{-/-};Sfrp2^{-/-}$ embryos, few traced axons take abnormal trajectories. Please note the increased number of RGCs in the double mutant (asterisk in **N**) as already described (Esteve et al., 2011b). Scale bars, 200 μm (**A–I**; **L–N**).
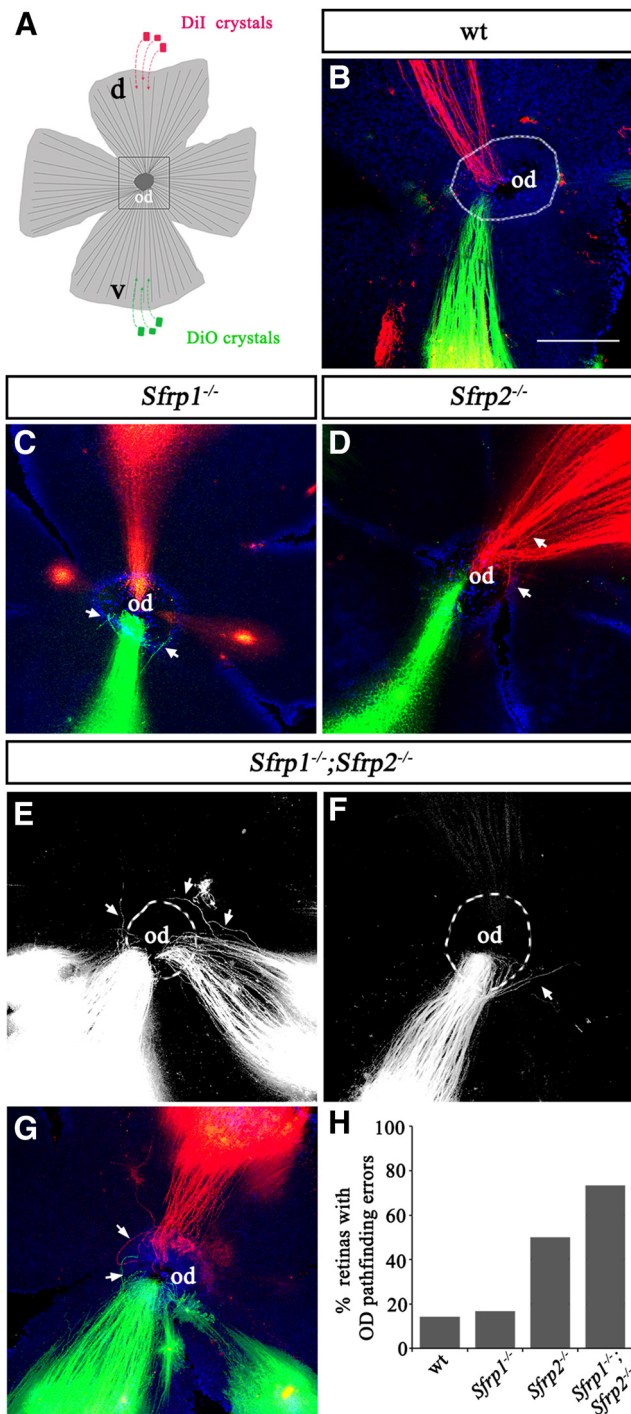
Figure 3. A proportion of RGC axons fail to enter the OD in the absence of *Sfrp2*. ***A***, Schematic representation of the tracing strategy using crystals of DiI (red) and DiO (green) in the dorsal (d) and ventral (v) retina, respectively. ***B–G***, Fluorescent images of flat-mounted preparations from E15.5 wt (***B***), *Sfrp1*$^{-/-}$ (***C***), *Sfrp2*$^{-/-}$ (***D***), and *Sfrp1*$^{-/-}$;*Sfrp2*$^{-/-}$ (***E–G***) retinas. Dashed lines indicate the position of the OD. Note that wt axons from the dorsal and ventral retina extend straight into the OD (***B***), whereas a small proportion of axons avoid the OD in mutants (arrows, ***C–G***). ***H***, Percentage of DiI- and DiO-labeled retinas with axons that fail to enter or detour around the OD in wt (n = 14), *Sfrp1*$^{-/-}$ (n = 36), *Sfrp2*$^{-/-}$ (n = 20), and *Sfrp1*$^{-/-}$;*Sfrp2*$^{-/-}$ (n = 30). Scale bars, 200 μm (***B–G***).

bundles grew away from the OD (Fig. 3*E–H*). These defects were more severe and frequent in the ventral retina (67% vs 33% dorsal). Notably, tracing uncovered similar, but less frequent, defects in *Sfrp2*$^{-/-}$ embryos (Fig. 3*D,H*), which had passed unnoticed in immunostained preparations (Fig. 2*E*).

Together, these results indicate that Sfrp2 and Sfrp1 influence the intraretinal growth of RGC axons by preventing axons to invade the deep layers of the retina and by fostering their turning into the OD. The prevalence of defects in the ventral retina likely reflects the enrichment of *Sfrp2* expression in these regions.

Sfrps are required for proper growth of RGC axons at the chiasm and tract regions

After leaving the OD, RGC axons navigate along the optic nerve toward the ventral midline of the diencephalon, where axons from the two eyes meet to form the optic chiasm. In mice, the majority of axons cross the midline and enter the contralateral optic tract, whereas a small proportion arising from the ventro-temporal RGCs remains uncrossed and projects into the ipsilateral tract (Petros et al., 2008). In contrast to the chick (Rodríguez et al., 2005), *Sfrp1* and *Sfrp2* were not expressed in the diencephalon, but they were found along the axons (Fig. 1*B,D,I,K*), prompting us to search for additional alterations.

Upon complete unilateral DiI filling of the optic nerve, RGC axons from E15.5 wt, *Sfrp1*$^{-/-}$, and *Sfrp2*$^{-/-}$ embryos showed a normal sorting behavior at the midline (Fig. 4*A–C*), with few fibers, slightly more abundant in the mutants, invading the contralateral optic nerve as reported previously (Plump et al., 2002; Sánchez-Camacho and Bovolenta, 2008). However, in *Sfrp2*$^{-/-}$ and *Sfrp1*$^{-/-}$;*Sfrp2*$^{-/-}$ embryos, a significant number of axons defasciculated prematurely at the distal end of the nerve and thereafter looped back into the chiasm (Fig. 4*C,D,H*), which appeared more loosely packed (Fig. 4*C–F*). This defect was more evident in *Sfrp1*$^{-/-}$;*Sfrp2*$^{-/-}$ embryos: in ~80% of the double mutants (n = 23), axons were dispersed in the anterior–posterior axis (Fig. 4*D*). In the remaining 20%, the chiasm showed a phenotype similar to that described for *Slit1*$^{-/-}$;*Slit2*$^{-/-}$ or *Robo2*$^{-/-}$ embryos (Plump et al., 2002; Plachez et al., 2008). Many disheveled fibers crossed the midline anterior to the chiasm, sometimes forming an additional bundle and with a few axons taking aberrant anterior routes (Fig. 4*E*). In the most extreme case, fibers appeared randomly distributed, equally dividing into the ipsilateral and contralateral tract and nerve (Fig. 4*F*). DiI tracings of the different genotypes at E13.5, when the first set of RGC axons reach the chiasm, demonstrated a mild anterior dispersion of RGC axons at the double mutant chiasm and a comparable organization of the axons in wt, *Sfrp1*$^{-/-}$, and *Sfrp2*$^{-/-}$ embryos (Fig. 4*G*). This indicates that late-born axons are more dependent on Sfrp-mediated axon fasciculation/guidance than early generated, pioneer axons.

Once they cross the midline, wt RGC axons extend along the tract in fasciculated bundles and fan out as they approach the LGN (Fig. 5*A*). In *Sfrp1*$^{-/-}$ and, more evidently, in *Sfrp2*$^{-/-}$ brains, this fanning was premature and its width significantly accentuated (Fig. 5*A–C,E–G,I*). In addition, some fibers aberrantly extended toward the dorsal diencephalon (Fig. 5*E–G,I*), as reported for *Robo2* mutants (Plachez et al., 2008). The latter behavior was more evident in compound mutants, possibly explaining why their optic tract "fan" was narrower than that of wt (Fig. 5*D,H–J*). This difference in width may also be explained by the presence of mediolateral defasciculation of the optic tract, which was evident upon brain sectioning (Fig. 5*K,L*). It may also in part reflect the shortening of the anteroposterior axis characteristic of double but not single Sfrp mutants (Satoh et al., 2006). Of note, the site of initial aberrant defasciculation of the optic tract, although similar among embryos of the same genotype, was distinct among the three genotypes (Fig. 5*A–D*, arrowheads),
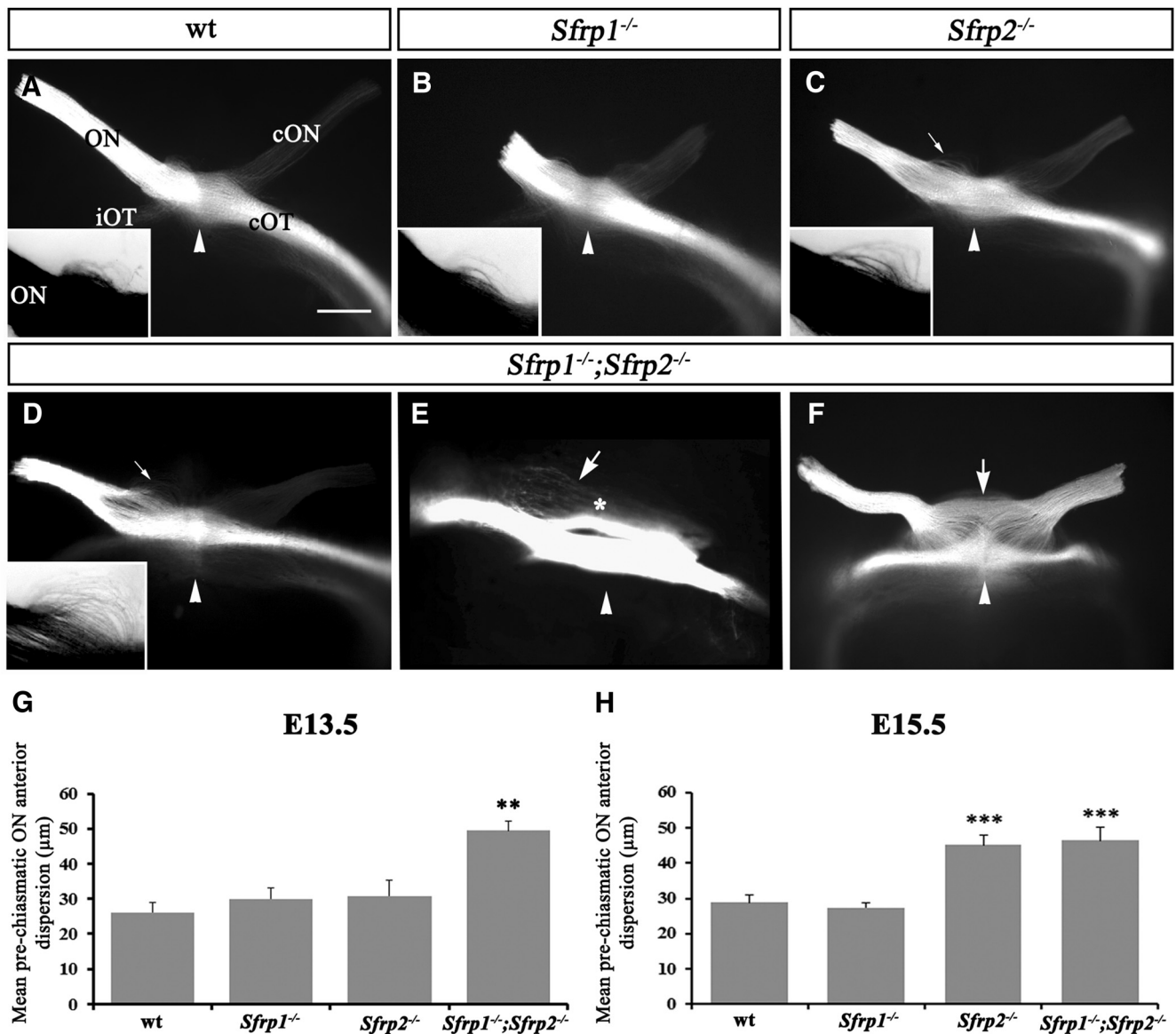
Figure 4. Sfrp's are required for proper growth of RGC axons at the chiasm. *A–F*, Ventral views of intact brain preparations from E15.5 wt (*A*), Sfrp1 $^{-/-}$ (*B*), Sfrp2 $^{-/-}$ (*C*), and Sfrp1 $^{-/-}$; Sfrp2 $^{-/-}$ (*D–F*) embryos. Axons from the right eye were traced by the insertion of DiI crystals into the OD. Anterior is to the top, posterior to the bottom. Arrowheads indicate the midline. Insets in *A–D* are high magnifications with inverted contrast of the prechiasmatic end of the optic nerve. In wt and Sfrp1 $^{-/-}$ (*A, B*), RGC axons extend into the optic nerve (ON) in tight bundles and slightly defasciculate as they enter the optic chiasm (inset). The majority of the axons enter the contralateral optic tract (cOT), whereas a small proportion remain uncrossed and grow into the ipsilateral optic tract (iOT) or enter the contralateral optic nerve (cON). The prechiasmatic end of the ON appears more defasciculated in Sfrp2 $^{-/-}$ and Sfrp1 $^{-/-}$; Sfrp2 $^{-/-}$ (arrows and insets in *C–E*). Note also the presence of small axon bundles (arrowhead in *E*). *F*, In extreme cases, fibers appear completely defasciculated, equally divided into the ipsilateral and contralateral tracts, with many axons entering the contralateral optic nerve. *G, H*, Mean ± SEM of the prechiasmatic dispersion of the optic nerve at E13.5 and E15.5. **$p < 0.01$; ***$p < 0.001$ compared with wt (Student's *t* test). Scale bars, 200 μm (*A–F*).

Sfrps influence compacted RGC axon growth with an ADAM10-dependent mechanism

Together, these data indicate that Sfrp's contribute both to intraretinal pathfinding of peripheral RGC axons and to fostering the organized growth of visual fibers along their pathway. Sfrp1 modulates mouse RGC axon growth (Sebastián-Serrano et al., 2012) and induces a bifunctional and extracellular matrix-dependent chemotropic turning response in chick and *Xenopus* RGC growth cones (Rodríguez et al., 2005). Therefore, Sfrp1 and Sfrp2, expressed in the retina and enriched at the OD (Fig. 1), likely act as intraretinal guidance cues, perhaps in combination

with extracellular matrix molecules. However, defects in regions of the pathway, in which there is no local Sfrp protein production, together with Sfrp protein localization along the RGC axons, suggested that an additional, perhaps autonomous mechanism might account for the axonal phenotype observed in *Sfrp* mutants.

Sfrp1 and Sfrp2 act as Wnt signaling inhibitors and thus their activity ultimately influences the expression of Wnt target genes (Bovolenta et al., 2008). We therefore considered the possibility that, in absence of *Sfrp1* and *Sfrp2*, the expression of axon guidance cues could be altered. Indeed, intraretinal defects related to those observed in Sfrp mutants have been reported in mice deficient in *EphB2*, *EphB3*, *Slit1/2*, *Robo2*, *BmpR1b*, and *Netrin1* (Deiner et al., 1997; Birgbauer et al., 2000; Liu et al., 2003b;
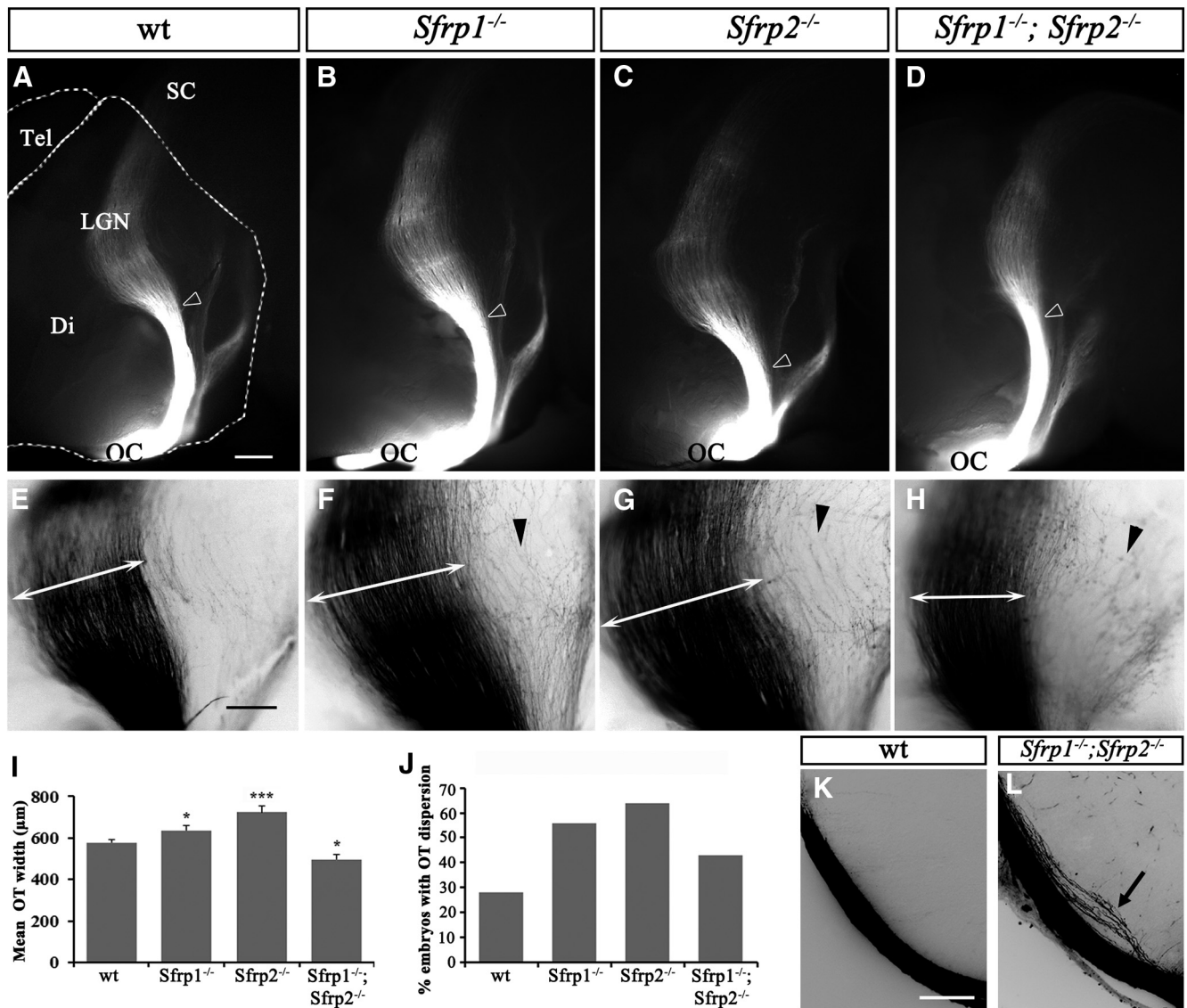
Figure 5. *Sfrp1* and *Sfrp2* deficiency causes premature defasciculation of axons in the optic tract. *A–H*, Lateral views of DiI-labeled RGC axons as they grow along the contralateral optic tract in whole brain preparations from E15.5 wt (*A, E*), *Sfrp1*⁻/⁻ (*B, F*), *Sfrp2*⁻/⁻ (*C, G*), and *Sfrp1*⁻/⁻; *Sfrp2*⁻/⁻ (*D, H*) embryos. The tract was exposed after cortex removal. In all images, dorsal is up and caudal is to the right. Open arrows in *A–D* point to the level in which the optic tract starts to fan out, which is slightly distinct among the genotypes. *E–H*, Images are higher magnifications at the level of the lateral geniculate nucleus (LGN) of those shown in *A–D*. The contrast has been inverted to better appreciate the caudal dispersion of labeled fibers (arrowheads). Double arrowed lines in *E–H* indicate the width occupied by DiI-labeled fibers as they approach the LGN. *I*, Mean ± SEM of the optic tract width in wt (*n* = 11), *Sfrp1*⁻/⁻ (*n* = 11), *Sfrp2*⁻/⁻ (*n* = 10), and *Sfrp1*⁻/⁻;*Sfrp2*⁻/⁻ (*n* = 11) embryos at the level indicated in *E–H*. *J*, Percentage of DiI-labeled wt and mutant embryos with an evident caudal spreading of the optic tract. *$p < 0.05$; ***$p < 0.001$ compared with wt (Student's *t* test). *K, L*, Fluorescent images with inverted contrast of frontal sections at the level of the optic tract from wt (*K*) and *Sfrp1*⁻/⁻;*Sfrp2*⁻/⁻ (*L*) E15.5 embryos after unilateral DiI filling of the visual fibers. Note the lateral to medial dispersion of the fibers in the compound mutants (arrow). Di, Diencephalon; OC, optic chiasm; SC, superior colliculus; Tel, telencephalon. Scale bars: 150 μm (*A–D*), 100 μm (*E–H*), 200 μm (*K, L*).

Thompson et al., 2006b; Plachez et al., 2008; Thompson et al., 2009) and after interference with RGC-derived Shh signaling (Kolpak et al., 2005; Sánchez-Camacho and Bovolenta, 2008). However, analysis of the mRNA distribution of *Netrin1*, *Shh*, *EphB2*, *Slit1*, *Slit2*, and *Robo2* in the eye of wt and *Sfrp1* and *Sfrp2* single and compound mutants revealed no significant differences (data not shown), suggesting that abnormal gene transcription was an unlikely cause of the observed phenotype.

We have previously shown that Sfrps act as negative modulators of ADAM10. Accordingly, the proteolysis of different ADAM10 substrates—Notch, APP, L1, and *N*-cadherin (Weber and Saftig, 2012)—is enhanced in *Sfrp*-null mice (Esteve et al., 2011b). *Adam10* mRNA, although expressed in the entire retinal neuroepithelium, was abundantly localized to the RGCs of both

wt and mutant E15.5 retinas (Fig. 6*A–C*) at similar levels, as also determined by semiquantitative RT-PCR analysis (data not shown). Therefore, Sfrp proteins localized to the RGC axons could control ADAM10 activity, which in turn would regulate, in an autonomous way, the shedding of membrane molecules involved in proper axon growth. If this were the case, the mode of outgrowth of retinal explants from wt or mutant embryos should be different. To test this possibility, we compared neurite outgrowth from E14.5 wt and single or compound mutant explants derived from different retinal quadrants to account for the non-homogeneous *Sfrp* distribution throughout the retinal neuroepithelium (Fig. 1). No significant difference in neurite length was observed between wt and mutants when outgrowth from each specific quadrant was compared, although there were intrinsic

outgrowth variations among quadrants (data not shown), as described previously (Marcus et al., 1996; Wang et al., 1996). Nevertheless, there was a consistent difference in the mode of outgrowth: explants from wt retinas in general extended arrays of tightly packed axonal bundles, whereas axons from $Sfrp2^{-/-}$ and $Sfrp1^{-/-};Sfrp2^{-/-}$ explants grew with a "sheet-like" appearance (Fig. 6D–F). High-power confocal analysis confirmed the preferential fasciculation of wt axons and the almost individual and disheveled growth of mutant axons (Fig. 6G–I), which was largely reverted upon addition of Sfrp1 protein to the culture medium (Fig. 6J–L). To quantify this behavior, we focused on $Sfrp1^{-/-};Sfrp2^{-/-}$ explants, which displayed the most evident phenotype. Measure of the mean width of wt and $Sfrp1^{-/-};Sfrp2^{-/-}$ axon fascicles confirmed that $Sfrp1^{-/-};Sfrp2^{-/-}$ axons formed significantly thinner fascicles than those formed by wt axons (22.56 ± 4 vs 34.4 ± 5.6 pixels, $p = 0.0418$; Fig. 6P). The addition of Sfrp1 protein to the culture medium had a mild effect on the fasciculation of wt axons but caused a significant increase of the fascicle width in $Sfrp1^{-/-};Sfrp2^{-/-}$ explants (30.4 ± 2.63 vs 22.56 ± 4 pixels, $p = 0.0153$) with a value close to that of wt explants ($p = 0.438$; Fig. 6P). Furthermore, the proportion of fascicles wider than 60 pixels in $Sfrp1^{-/-};Sfrp2^{-/-}$ explants was ~3-fold less than that observed in wt explants (5.8% and 14.3% respectively), but Sfrp1 addition neared their fasciculation score to that observed in wt (14.37%; Fig. 6Q). A similar trend was observed upon addition of the ADAM10-specific inhibitor GI254023X (5 µM; Fig. 6M–O), which made the outgrowth of $Sfrp2^{-/-}$ retinal explants (13.53 ± 0.70)—taken as an example—comparable to that of wt (20.10 ± 1.10 vs 21.95 ± 1.82, $p = 0.54$; Fig. 6R), increasing the proportion of wider fascicles to values similar to that of wt (Fig. 6S).

All in all, these data suggest that Sfrp proteins favor the fasciculated growth of RGC axons with a mechanism that implicates ADAM10. A recent study showed that *Drosophila* ADAM10/Kuzbanian is involved in Robo receptor activation (Coleman et al., 2010) and Sfrp1 interferes with Kuzbanian activity (Esteve et al., 2011b). Given the expression of Robos in RGCs and the similarity in the phenotypic traits of $Sfrp2^{-/-}$, $Sfrp1^{-/-};Sfrp2^{-/-}$ and *Robo2/Slit* mutants (Plump et al., 2002; Thompson et al., 2006a; Thompson et al., 2009), we first considered the possibility that ADAM10-mediated
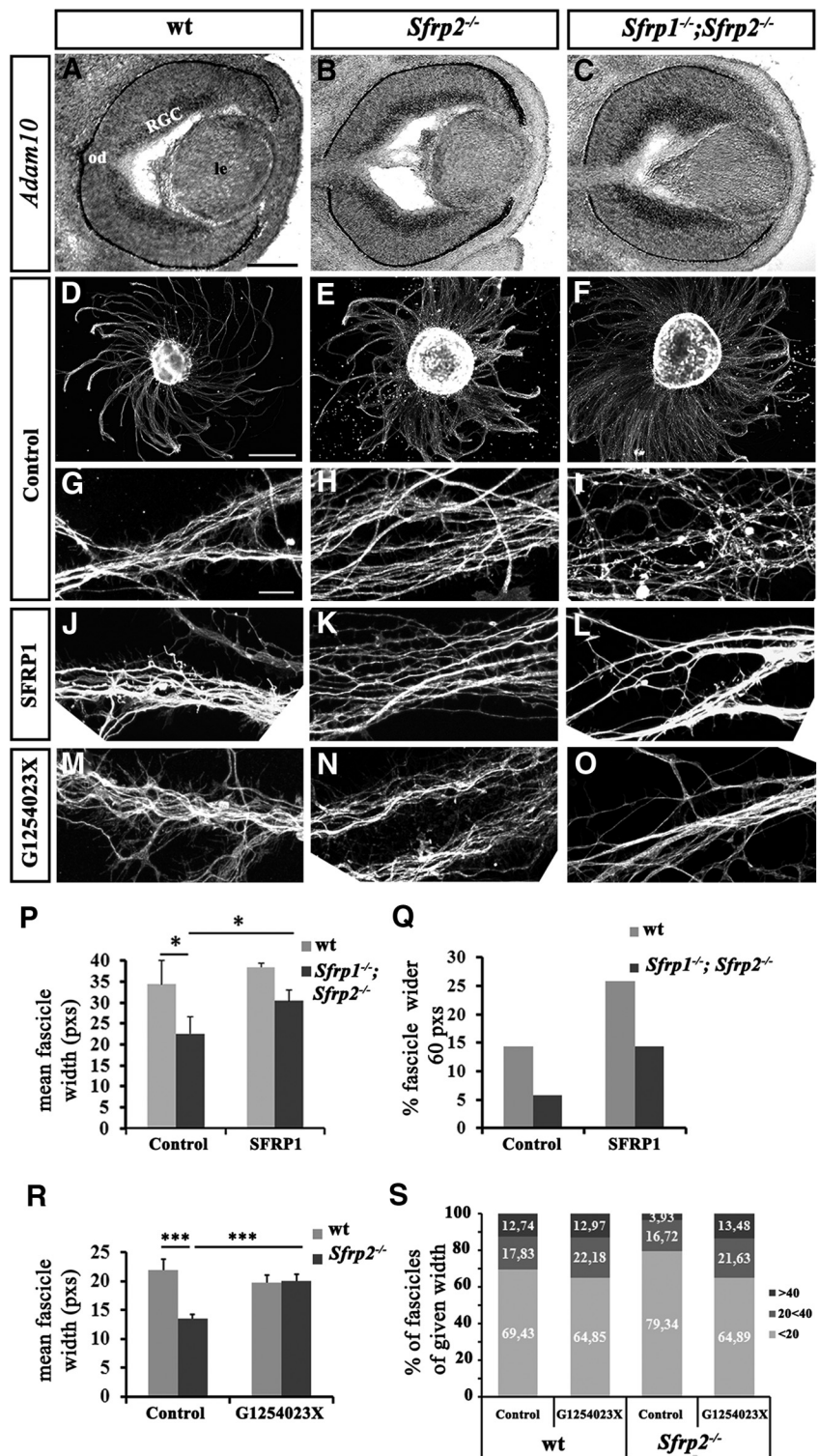

Figure 6. Fasciculated growth of RGC neurites requires modulation of ADAM activity by Sfrp's. ***A–C***, Transverse sections of E15.5 retinas from wt, $Sfrp2^{-/-}$ and $Sfrp1^{-/-};Sfrp2^{-/-}$ embryos hybridized with a probe against *Adam10*. Note the strong *Adam10* expression in the RGC layer. In double mutants, the number of RGCs is increased as described previously (Esteve et al., 2011a). ***D–O***, Low- and high-power views of retinal explants from E15.5 wt (***D, G, J, M***), $Sfrp2^{-/-}$ (***E, H, K, N***) and $Sfrp1^{-/-};Sfrp2^{-/-}$ (***F, I, L, O***) embryos cultured alone (***D–I***) or in the presence of Sfrp1 protein (***J–L***) or GI254023X, a specific ADAM10 inhibitor (***M–O***). ***P***, Mean ± SEM width of neurite fascicles of retinal explants from wt or $Sfrp1^{-/-};Sfrp2^{-/-}$ embryos cultured in different conditions. ***Q***, Graph representing the proportion of fascicles wider than 60 pixels (pxs) in wt and $Sfrp1^{-/-};Sfrp2^{-/-}$ retinal explants grown with or without the addition of Sfrp1. ***R***, Mean ± SEM width of neurite fascicles of retinal explants from wt or $Sfrp2^{-/-}$ retinas grown with DMSO (control) or GI254023X. ***S***, Graph representing the proportion of fascicles of given width from wt and $Sfrp2^{-/-}$ retinal explants grown with DMSO or GI254023X. *$p < 0.05$; ***$p < 0.001$, Student's *t* test. Scale bars: 200 µm (***A–C***), 200 µm (***D–F***), 10 µm (***G–O***).
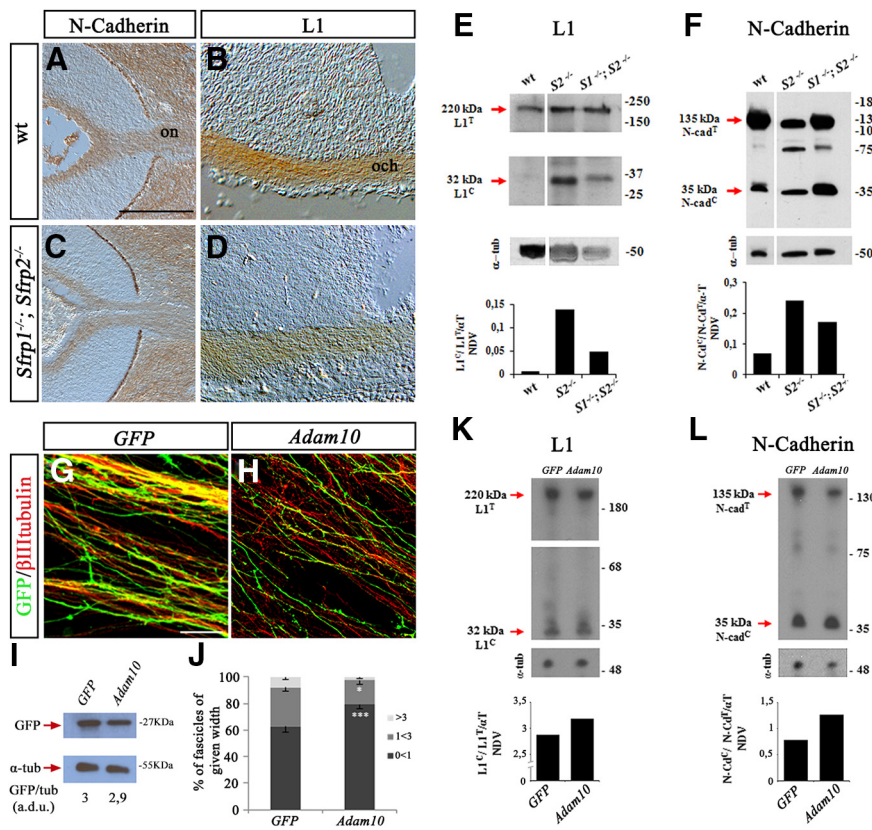
Figure 7. ADAM10 mediates disheveled RGC axon growth likely by regulating L1 and N-cadherin proteolysis. *A–D*, Transverse sections of E15.5 wt (*A*, *B*) and *Sfrp1* $^{-/-}$;*Sfrp2* $^{-/-}$ (*C*, *D*) embryos at the level of the eye (*A*, *C*) and optic chiasm (*B*, *D*). Sections are immunostained with α-N-cadherin (*A*, *C*) and α-L1 (*B*, *D*) antibodies. *E*, *F*, Western blot analysis of L1 (*E*) and N-cadherin (*F*) processing in lysates of the proximal visual pathway from E16.5 wt, *Sfrp2* $^{-/-}$, and *Sfrp1* $^{-/-}$;*Sfrp2* $^{-/-}$ embryos. The 32 kDa L1 and 35 kDa N-cadherin fragments are increased in *Sfrp2* $^{-/-}$ and *Sfrp1* $^{-/-}$;*Sfrp2* $^{-/-}$ embryos, as shown in the graph bar representation of processed and unprocessed bands normalized to α-tubulin as a loading control. The data represent a typical experiment. The lane showing the wt lysate derives from the same gel, in which an intermediate lane was eliminated. *G*, *H*, Confocal images of the retinal explants electroporated with *GFP* (*G*) or *GFP* + *Adam10* (*H*)-immunostained with antibodies against GFP and β-III-tubulin. Note that ADAM10 overexpression causes axon defasciculation. *I*, Western blot analysis of GFP demonstrating similar levels of explant targeting. GFP levels were normalized against α-tubulin. *J*, Graph representing the proportion of fascicles of given width from retinal explants electroporated with *GFP* or *Adam10*. ADAM10 significantly reduces the number of wider fascicles. *K*, *L*, Western blot analysis of L1 (*K*) and N-cadherin (*L*) processing in lysates of *GFP* and *Adam10*-electroporated retinal explants. Note the increased ratio of processed/unprocessed N-cadherin and L1 normalized to α-tubulin in *Adam10*-overexpressing explants. on, Optic nerve; och (optic chiasm). *p < 0.05, ***p < 0.001; Bonferroni's test. Scale bars: 200 μm (*A–D*), 10 μm (*G–H*).

Robo processing would be conserved in mammals and that its shedding would be increased in absence of Sfrp proteins. However, experiments with *Robo2*- and *Adam10*-transfected cell lines, as well as Western blot analysis of embryonic visual pathway lysates from wt and *Sfrp*-null genotypes did not reveal significant Robo2 processing (data not shown). We next analyzed whether N-cadherin and L1, two ADAM10-specific substrates (Reiss et al., 2005; Riedle et al., 2009) previously implicated in selective fasciculation of visual axons (Riehl et al., 1996; Mi et al., 1998; Lyckman et al., 2000; Masai et al., 2003), presented an enhanced proteolytical processing in the visual pathway of *Sfrp1* $^{-/-}$;*Sfrp2* $^{-/-}$ mice, as previously observed in retinal tissue (Esteve et al., 2011b). Both molecules are strongly expressed in wt and *Sfrp1* $^{-/-}$;*Sfrp2* $^{-/-}$ E15.5 RGC axons (Fig. 7A–D), so their abnormal processing could collectively explain the *in vivo* and *in vitro* phenotype observed in Sfrp mutants. ADAM10 sheds the extracellular domain of L1 and N-cadherin and this is prerequisite for further proteolysis by a γ-secretase, which generates intracellular peptides of 35 kDa for N-cadherin and 28 kDa for L1 (Reiss et al., 2005; Riedle et

al., 2009). Western blot analysis of the relative proportion of these fragments from the isolated proximal visual pathway (from the retina to the LGN) of E16.5 wt, *Sfrp2* $^{-/-}$, and *Sfrp1* $^{-/-}$;*Sfrp2* $^{-/-}$ embryos revealed an increased shedding of L1 and N-cadherin in *Sfrp2* $^{-/-}$ and *Sfrp1* $^{-/-}$;*Sfrp2* $^{-/-}$ mutants compared with wt (Fig. 7E,F). Therefore, as demonstrated previously (Esteve et al., 2011b), genetic inactivation of Sfrp proteins seemed to increase ADAM10 activity, which likely impinged upon the fasciculated growth of RGC axons. If this were the case, then overexpression of ADAM10 in retinal explants should mimic the behavior of Sfrp mutant retinas. Indeed, electroporation of equal amounts of plasmids carrying either GFP or *Adam10* demonstrated that ADAM10-overexpressing axons extended rather independently, in contrast to control GFP-expressing axons, which formed small fascicles (Fig. 7G–J). This behavior was associated with an increased proteolysis of N-cadherin and L1 in *Adam10*-overexpressing explants (Fig. 7K,L), although this was less pronounced than that observed in *Sfrp* mutants (Fig. 7E,F), likely because only a proportion of RGCs are targeted by the electroporation.

Altogether, these data support the possibility that defasciculation defects observed in the absence of Sfrp1/2 are a consequence of abnormal ADAM10-mediated processing, at least of N-cadherin.

Discussion

Axon growth depends on the interplay of different molecular signals. Multifunctionality of one or few of such signals may be an efficient way of ensuring coordinated information. Shh signaling acting on spinal cord commissural axons is an example. Indeed, Shh secreted by the floor plate attract precrossing axons at the ventral midline and thereafter repel postcrossing axons to favor their anterior longitudinal growth (for review, see Bovolenta, 2005). At the same time, it ensures that axons acquire responsiveness to Semaphorin (Parra and Zou, 2010), a cue that also helps axons out of the midline (Nawabi et al., 2010). In the chick spinal cord, Shh signaling further controls the ventral expression of *Sfrp1*, which shapes the gradient of Wnt proteins that promote the longitudinal growth of commissural axons (Domanitskaya et al., 2010). In a different paradigm, we have shown here that Sfrp proteins are required for preventing RGC axons to invade the deep layers of the retina and to constrain their growth into the OD, likely with a direct mechanism (Rodríguez et al., 2005). At the same time, Sfrp's are needed to promote cohesive axon extension by ensuring the appropriate ADAM10-mediated shedding of cell adhesion molecules, further demonstrating that fine regulation of metalloproteinases is critical to coordinating the development of neuronal projections (McFarlane, 2003; Bai and Pfaff, 2011).

These conclusions are based on the analysis of single and compound *Sfrp1* and *Sfrp2* mouse mutants, which showed mild but

consistent defects in intraretinal pathfinding and fiber fasciculation. *Sfrp1* and *Sfrp2* are expressed with different and restricted patterns, but, consistent with their diffusible nature, immunostaining shows that Sfrp proteins localize more broadly than their mRNA, as reported in previous studies (Mii and Taira, 2009; Esteve et al., 2011a) and possibly explaining their functional redundancy (Satoh et al., 2006; Esteve et al., 2011b). Consistent with this redundancy, compound *Sfrp1$^{-/-}$;Sfrp2$^{-/-}$* mutants had the strongest phenotype, followed by *Sfrp2$^{-/-}$* embryos, whereas only subtle defects were observed in the *Sfrp1$^{-/-}$* mutants. Shortening of the anteroposterior axis, lack of retinal periphery, and increased number of RGCs found in compound mutants (Satoh et al., 2006; Esteve et al., 2011a; Esteve et al., 2011b) may influence their axon phenotype. However, similar patterning defects were never observed in the *Sfrp2$^{-/-}$* mutants (Satoh et al., 2006; Esteve et al., 2011a; Esteve et al., 2011b), which show a similar visual pathway phenotype, making this possibility unlikely. In addition, analysis of brain patterning of single and compound *Sfrp1* and *Sfrp2* mutants revealed predominant dorsal defects (I. Crespo, A.S., P.B., and P.E., unpublished data), compatible with their reported pallial and subpallial expression (Leimeister et al., 1998; Kim et al., 2001). In contrast, the retinal distribution of Sfrp2 and, to a lesser extent, of Sfrp1, indicates that, normally, these proteins prevent RGC axons from invading the deep layers of the retinas. As a result, in *Sfrp2$^{-/-}$* and *Sfrp1$^{-/-}$; Sfrp2$^{-/-}$* compound mutant embryos, a subset of ventroperipheral RGC axons no longer stray away from the outer layers of the retina, resembling the defects described for *Robo2* and *Slit1* and *Slit2* compound mutants (Plump et al., 2002; Plachez et al., 2008). Similarly, the relative abundance of *Sfrp2* at the OD, which is fundamental for guiding axons out of the eye (Morcillo et al., 2006), explains the defects of outgrowth observed in this region in both *Sfrp2* and compound mutants. OD-derived Sfrp's, in combination with laminin localized to the optic nerve head (Höpker et al., 1999), may directly signal at the RGC growth cones forcing the axons to enter the OD. This mechanism would be similar to what has been shown for the combination of Netrin1 and laminin (Höpker et al., 1999) or proposed for laminin/EphB (Birgbauer et al., 2000; Suh et al., 2004). This is also in agreement with the observation that chick and *Xenopus* RGC axons are uniformly and strongly repelled by the combination of Sfrp1 and laminin in both turning and stripe assays and exposed brain preparations in which Sfrp1 addition deviates visual axon trajectory in regions of the optic tract, in which laminin is particularly abundant (Rodríguez et al., 2005).

Sfrp's are not expressed in region surrounding the visual pathway, suggesting that Sfrp proteins localized to the RGC axons could explain, in an autonomous way, the defects observed in the chiasm and optic tract region. Our data support this possibility, suggesting that abnormal RGC axon growth might in part be a consequence of an increased activity of ADAM10- abundantly expressed by RGCs caused by *Sfrp1* and *Sfrp2* genetic inactivation. In tissue culture, explants from Sfrp-null animals grow with a disheveled appearance, which is attenuated by the addition of either Sfrp1 or a specific inhibitor of ADAM10 metalloproteinase activity. Furthermore, electroporation of *Adam10* in retinal explants promotes a poorly cohesive growth of targeted axons that thus behave similarly to those of Sfrp mutant retinas. Shedding of L1 and N-cadherin, two of the multiple ADAM10 substrates, is increased in the visual pathway of *Sfrp*-null mice and in wt retinal explants overexpressing *Adam10*, although in the latter case, to a lesser extent because only a proportion of RGCs are targeted by electroporation. This abnormal processing may contribute to the

disheveled axon growth observed in both experimental paradigms. Supporting this possibility, L1 and N-cadherin have been involved in homophilic and heterophilic interactions (Hivert et al., 2002; Bao, 2008) and alteration of their expression causes visual axon defects resembling those observed in *Sfrp* mutants (Bastmeyer et al., 1995; Riehl et al., 1996; Mi et al., 1998; Lyckman et al., 2000; Masai et al., 2003). We cannot, however, exclude that abnormal processing of other guidance cues may contribute to the phenotypes we are describing. Although we could not demonstrate a role for ADAM10 in vertebrate Robo2 shedding, the Robo/Slit signaling system is still a good candidate, perhaps implicating the processing of Slits or a different Sfrp-modulated metalloproteinase (Bovolenta et al., 2008; also see below). In fact, *Sfrp2$^{-/-}$*, *Sfrp1$^{-/-}$;Sfrp2$^{-/-}$*, *Robo2*, and *Slit* mutants share phenotypic traits (Plump et al., 2002; Thompson et al., 2006a; Thompson et al., 2009) and Slit-mediated activation of Robo2 has been implicated in axon fasciculation (Jaworski and Tessier-Lavigne, 2012). Furthermore, Robo receptors undergo homophilic interactions (Hivert et al., 2002) and have been implicated in zebrafish visual axon fasciculation (Devine and Key, 2008). Other molecules that we have not tested are also possible additional candidates: the Eph-Ephrin signaling pair is an example because these molecules are established ADAM10 substrates (Weber and Saftig, 2012) that contribute to intraretinal axon fasciculation (Mühleisen et al., 2006). A recent report has also suggested that ADAM proteinases participate in the shedding of Shh from the producing cells (Ohlig et al., 2011). Notably, interference with RGC-derived Shh causes intraretinal defects similar to those observed in *Sfrp1/2* mutants (Kolpak et al., 2005; Sánchez-Camacho and Bovolenta, 2008) and blockage of Shh signaling in *Xenopus* leads to defasciculation of the caudal optic tract (Gordon et al., 2010). Similarly, the Netrin1 receptor DCC, crucial for RGC axons navigation at the optic nerve head (Deiner et al., 1997), is shed by a metalloproteinase (Galko and Tessier-Lavigne, 2000).

Our study does not clearly establish whether ADAM10 is uniquely responsible for the disheveled growth observed in Sfrp mutants. The singularity of Sfrp/ADAM10 binding has not been addressed (Esteve et al., 2011b), so Sfrp proteins may interfere with other metalloproteinases. Indeed, although *Adam10* is the only ADAM family member enriched in RGCs, ADAM11, ADAM17, and ADAM28 are also found in the retina.

We propose a dual function for Sfrp1/2 in the guidance of RGC axons, but the phenotype resulting from the inactivation of one or both molecules is, perhaps surprisingly, mild and sometimes incompletely penetrant for these combined effects. There are several possible, diverse reasons. For example, the absence of Sfrp1/2 at the OD might be compensated by the presence of Netrin or EphB (Deiner et al., 1997; Birgbauer et al., 2000). *Sfrp5*, the member of the Sfrp family most closely related to *Sfrp1* and *Sfrp2* (Bovolenta et al., 2008), is expressed in the developing eye (Chang et al., 1999; Ruiz et al., 2009) and may in part compensate for *Sfrp1/2* deficiency. Furthermore, and likely more relevant, shedding of guidance cues should be considered as an ultimate layer of regulation that fine-tunes axon navigation and enhances its fidelity (Bai and Pfaff, 2011).

In conclusion, our study adds new evidence of the multiple roles that Sfrp proteins play in both development and adult tissue homeostasis (Esteve and Bovolenta, 2010). These functions are context dependent and may vary according to their localization, level of expression, and interaction with other molecules. The role of Sfrp proteins as modulators of shedding events is particularly intriguing because protein shedding regulates many basic

events in addition to axon guidance. These include cell adhesion, cell migration, inflammatory events or signaling activation, and extinction. Furthermore, sheddase-regulated proteins are expressed not only during initial brain wiring, but persist in the adult CNS and participate in the maintenance, repair, and plasticity of neural circuits (Saxena and Caroni, 2007). Our finding, therefore, might have important implications in neurodegenerative diseases or in vasculature formation, a process that is controlled by similar sets of molecules (Jones and Li, 2007). In this respect, it is interesting to note that *Sfrp* mutant mice have evident vasculature defects (Esteve et al., 2011b).

References

Bai G, Pfaff SL (2011) Protease regulation: the Yin and Yang of neural development and disease. Neuron 72:9–21. CrossRef Medline

Bao ZZ (2008) Intraretinal projection of retinal ganglion cell axons as a model system for studying axon navigation. Brain Res 1192:165–177. CrossRef Medline

Bastmeyer M, Ott H, Leppert CA, Stuermer CA (1995) Fish E587 glycoprotein, a member of the L1 family of cell adhesion molecules, participates in axonal fasciculation and the age-related order of ganglion cell axons in the goldfish retina. J Cell Biol 130:969–976. CrossRef Medline

Birgbauer E, Cowan CA, Sretavan DW, Henkemeyer M (2000) Kinase independent function of EphB receptors in retinal axon pathfinding to the optic disc from dorsal but not ventral retina. Development 127:1231–1241. Medline

Blackshaw S, Harpavat S, Trimarchi J, Cai L, Huang H, Kuo WP, Weber G, Lee K, Fraioli RE, Cho SH, Yung R, Asch E, Ohno-Machado L, Wong WH, Cepko CL (2004) Genomic analysis of mouse retinal development. PLoS Biol 2:E247. CrossRef Medline

Bovolenta P (2005) Morphogen signaling at the vertebrate growth cone: a few cases or a general strategy? J Neurobiol 64:405–416. CrossRef Medline

Bovolenta P, Mason C (1987) Growth cone morphology varies with position in the developing mouse visual pathway from retina to first targets. J Neurosci 7:1447–1460. Medline

Bovolenta P, Esteve P, Ruiz JM, Cisneros E, Lopez-Rios J (2008) Beyond Wnt inhibition: new functions of secreted Frizzled-related proteins in development and disease. J Cell Sci 121:737–746. CrossRef Medline

Chang JT, Esumi N, Moore K, Li Y, Zhang S, Chew C, Goodman B, Rattner A, Moody S, Stetten G, Campochiaro PA, Zack DJ (1999) Cloning and characterization of a secreted frizzled-related protein that is expressed by the retinal pigment epithelium. Hum Mol Genet 8:575–583. CrossRef Medline

Coleman HA, Labrador JP, Chance RK, Bashaw GJ (2010) The Adam family metalloprotease Kuzbanian regulates the cleavage of the roundabout receptor to control axon repulsion at the midline. Development 137:2417–2426. CrossRef Medline

Deiner MS, Kennedy TE, Fazeli A, Serafini T, Tessier-Lavigne M, Sretavan DW (1997) Netrin-1 and DCC mediate axon guidance locally at the optic disc: loss of function leads to optic nerve hypoplasia. Neuron 19:575–589. CrossRef Medline

Devine CA, Key B (2008) Robo-Slit interactions regulate longitudinal axon pathfinding in the embryonic vertebrate brain. Dev Biol 313:371–383. CrossRef Medline

Domanitskaya E, Wacker A, Mauti O, Baeriswyl T, Esteve P, Bovolenta P, Stoeckli ET (2010) Sonic hedgehog guides post-crossing commissural axons both directly and indirectly by regulating Wnt activity. J Neurosci 30:11167–11176. CrossRef Medline

Erskine L, Herrera E (2014) Connecting the retina to the brain. ASN Neuro 6:pii:1759091414562107.

Esteve P, Bovolenta P (2010) The advantages and disadvantages of sfrp1 and sfrp2 expression in pathological events. The Tohoku Journal of Experimental Medicine 221:11–17. CrossRef Medline

Esteve P, Trousse F, Rodríguez J, Bovolenta P (2003) SFRP1 modulates retina cell differentiation through a beta-catenin-independent mechanism. J Cell Sci 116:2471–2481. CrossRef Medline

Esteve P, Lopez-Rios J, Bovolenta P (2004) SFRP1 is required for the proper establishment of the eye field in the medaka fish. Mech Dev 121:687–701. CrossRef Medline

Esteve P, Sandonìs A, Ibañez C, Shimono A, Guerrero I, Bovolenta P (2011a) Secreted frizzled-related proteins are required for Wnt/beta-catenin signalling activation in the vertebrate optic cup. Development 138:4179–4184. CrossRef Medline

Esteve P, Sandonìs A, Cardozo M, Malapeira J, Ibañez C, Crespo I, Marcos S, Gonzalez-Garcia S, Toribio ML, Arribas J, Shimono A, Guerrero I, Bovolenta P (2011b) Sfrp's act as negative modulators of ADAM10 to regulate retinal neurogenesis. Nat Neurosci 14:562–569. CrossRef Medline

Galko MJ, Tessier-Lavigne M (2000) Function of an axonal chemoattractant modulated by metalloprotease activity. Science 289:1365–1367. CrossRef Medline

Gordon L, Mansh M, Kinsman H, Morris AR (2010) *Xenopus* sonic hedgehog guides retinal axons along the optic tract. Dev Dyn 239:2921–2932. CrossRef Medline

Hattori M, Osterfield M, Flanagan JG (2000) Regulated cleavage of a contact-mediated axon repellent. Science 289:1360–1365. CrossRef Medline

Hauck SM, Hofmaier F, Dietter J, Swadzba ME, Blindert M, Amann B, Behler J, Kremmer E, Ueffing M, Deeg CA (2012) Label-free LC-MSMS analysis of vitreous from autoimmune uveitis reveals a significant decrease in secreted Wnt signalling inhibitors DKK3 and SFRP2. J Proteomics 75:4545–4554. CrossRef Medline

Hivert B, Liu Z, Chuang CY, Doherty P, Sundaresan V (2002) Robo1 and Robo2 are homophilic binding molecules that promote axonal growth. Mol Cell Neurosci 21:534–545. CrossRef Medline

Höpker VH, Shewan D, Tessier-Lavigne M, Poo M, Holt C (1999) Growth-cone attraction to netrin-1 is converted to repulsion by laminin-1. Nature 401:69–73. CrossRef Medline

Jaworski A, Tessier-Lavigne M (2012) Autocrine/juxtaparacrine regulation of axon fasciculation by Slit-Robo signaling. Nat Neurosci 15:367–369. CrossRef Medline

Jones CA, Li DY (2007) Common cues regulate neural and vascular patterning. Curr Opin Genet Dev 17:332–336. CrossRef Medline

Kim AS, Lowenstein DH, Pleasure SJ (2001) Wnt receptors and Wnt inhibitors are expressed in gradients in the developing telencephalon. Mech Dev 103:167–172. CrossRef Medline

Kobayashi K, Luo M, Zhang Y, Wilkes DC, Ge G, Grieskamp T, Yamada C, Liu TC, Huang G, Basson CT, Kispert A, Greenspan DS, Sato TN (2009) Secreted Frizzled-related protein 2 is a procollagen C proteinase enhancer with a role in fibrosis associated with myocardial infarction. Nat Cell Biol 11:46–55. CrossRef Medline

Kolpak A, Zhang J, Bao ZZ (2005) Sonic hedgehog has a dual effect on the growth of retinal ganglion axons depending on its concentration. J Neurosci 25:3432–3441. CrossRef Medline

Lee HX, Ambrosio AL, Reversade B, De Robertis EM (2006) Embryonic dorsal-ventral signaling: secreted frizzled-related proteins as inhibitors of tolloid proteinases. Cell 124:147–159. CrossRef Medline

Leimeister C, Bach A, Gessler M (1998) Developmental expression patterns of mouse sFRP genes encoding members of the secreted frizzled related protein family. Mech Dev 75:29–42. CrossRef Medline

Lemmon V, Farr KL, Lagenaur C (1989) L1-mediated axon outgrowth occurs via a homophilic binding mechanism. Neuron 2:1597–1603. CrossRef Medline

Lin CT, Lin YT, Kuo TF (2007) Investigation of mRNA expression for secreted frizzled-related protein 2 (sFRP2) in chick embryos. J Reprod Dev 53:801–810. CrossRef Medline

Liu H, Mohamed O, Dufort D, Wallace VA (2003a) Characterization of Wnt signaling components and activation of the Wnt canonical pathway in the murine retina. Dev Dyn 227:323–334. CrossRef Medline

Liu J, Wilson S, Reh T (2003b) BMP receptor 1b is required for axon guidance and cell survival in the developing retina. Dev Biol 256:34–48. CrossRef Medline

Ludwig A, Hundhausen C, Lambert MH, Broadway N, Andrews RC, Bickett DM, Leesnitzer MA, Becherer JD (2005) Metalloproteinase inhibitors for the disintegrin-like metalloproteinases ADAM10 and ADAM17 that differentially block constitutive and phorbol ester-inducible shedding of cell surface molecules. Combinatorial Chemistry and High-Throughput Screening 8:161–171. CrossRef Medline

Lyckman AW, Moya KL, Confaloni A, Jhaveri S (2000) Early postnatal expression of L1 by retinal fibers in the optic tract and synaptic targets of the Syrian hamster. J Comp Neurol 423:40–51. Medline

Malinverno M, Carta M, Epis R, Marcello E, Verpelli C, Cattabeni F, Sala C, Mulle C, Di Luca M, Gardoni F (2010) Synaptic localization and activity

of ADAM10 regulate excitatory synapses through N-cadherin cleavage. J Neurosci 30:16343–16355. Medline

Marcos S, Backer S, Causeret F, Tessier-Lavigne M, Bloch-Gallego E (2009) Differential roles of Netrin-1 and its receptor DCC in inferior olivary neuron migration. Mol Cell Neurosci 41:429–439. CrossRef Medline

Marcus RC, Wang LC, Mason CA (1996) Retinal axon divergence in the optic chiasm: midline cells are unaffected by the albino mutation. Development 122:859–868. Medline

Masai I, Lele Z, Yamaguchi M, Komori A, Nakata A, Nishiwaki Y, Wada H, Tanaka H, Nojima Y, Hammerschmidt M, Wilson SW, Okamoto H (2003) N-cadherin mediates retinal lamination, maintenance of forebrain compartments and patterning of retinal neurites. Development 130:2479–2494. CrossRef Medline

McFarlane S (2003) Metalloproteases: carving out a role in axon guidance. Neuron 37:559–562. CrossRef Medline

Mi ZP, Weng W, Hankin MH, Narayanan V, Lagenaur CF (1998) Maturational changes in cell surface antigen expression in the mouse retina and optic pathway. Brain Res Dev Brain Res 106:145–154. CrossRef Medline

Mii Y, Taira M (2009) Secreted Frizzled-related proteins enhance the diffusion of Wnt ligands and expand their signalling range. Development 136:4083–4088. CrossRef Medline

Morcillo J, Martínez-Morales JR, Trousse F, Fermin Y, Sowden JC, Bovolenta P (2006) Proper patterning of the optic fissure requires the sequential activity of BMP7 and SHH. Development 133:3179–3190. CrossRef Medline

Mühleisen TW, Agoston Z, Schulte D (2006) Retroviral misexpression of cVax disturbs retinal ganglion cell axon fasciculation and intraretinal pathfinding in vivo and guidance of nasal ganglion cell axons in vivo. Dev Biol 297:59–73. CrossRef Medline

Muraoka O, Shimizu T, Yabe T, Nojima H, Bae YK, Hashimoto H, Hibi M (2006) Sizzled controls dorso-ventral polarity by repressing cleavage of the Chordin protein. Nat Cell Biol 8:329–338. CrossRef Medline

Nawabi H, Briançon-Marjollet A, Clark C, Sanyas I, Takamatsu H, Okuno T, Kumanogoh A, Bozon M, Takeshima K, Yoshida Y, Moret F, Abouzid K, Castellani V (2010) A midline switch of receptor processing regulates commissural axon guidance in vertebrates. Genes Dev 24:396–410. CrossRef Medline

Ohlig S, Farshi P, Pickhinke U, van den Boom J, Höing S, Jakuschev S, Hoffmann D, Dreier R, Schöler HR, Dierker T, Bordych C, Grobe K (2011) Sonic hedgehog shedding results in functional activation of the solubilized protein. Dev Cell 20:764–774. CrossRef Medline

Parra LM, Zou Y (2010) Sonic hedgehog induces response of commissural axons to Semaphorin repulsion during midline crossing. Nat Neurosci 13:29–35. CrossRef Medline

Petros TJ, Rebsam A, Mason CA (2008) Retinal axon growth at the optic chiasm: to cross or not to cross. Annu Rev Neurosci 31:295–315. CrossRef Medline

Plachez C, Andrews W, Liapi A, Knoell B, Drescher U, Mankoo B, Zhe L, Mambetisaeva E, Annan A, Bannister L, Parnavelas JG, Richards LJ, Sundaresan V (2008) Robos are required for the correct targeting of retinal ganglion cell axons in the visual pathway of the brain. Mol Cell Neurosci 37:719–730. CrossRef Medline

Plump AS, Erskine L, Sabatier C, Brose K, Epstein CJ, Goodman CS, Mason CA, Tessier-Lavigne M (2002) Slit1 and Slit2 cooperate to prevent premature midline crossing of retinal axons in the mouse visual system. Neuron 33:219–232. CrossRef Medline

Reiss K, Maretzky T, Ludwig A, Tousseyn T, de Strooper B, Hartmann D, Saftig P (2005) ADAM10 cleavage of N-cadherin and regulation of cell-cell adhesion and beta-catenin nuclear signalling. EMBO J 24:742–752. CrossRef Medline

Riedle S, Kiefel H, Gast D, Bondong S, Wolterink S, Gutwein P, Altevogt P (2009) Nuclear translocation and signalling of L1-CAM in human carcinoma cells requires ADAM10 and presenilin/gamma-secretase activity. Biochem J 420:391–402. CrossRef Medline

Riehl R, Johnson K, Bradley R, Grunwald GB, Cornel E, Lilienbaum A, Holt CE (1996) Cadherin function is required for axon outgrowth in retinal ganglion cells in vivo. Neuron 17:837–848. CrossRef Medline

Rodríguez J, Esteve P, Weinl C, Ruiz JM, Fermin Y, Trousse F, Dwivedy A, Holt C, Bovolenta P (2005) SFRP1 regulates the growth of retinal ganglion cell axons through the Fz2 receptor. Nat Neurosci 8:1301–1309. CrossRef Medline

Romi E, Gokhman I, Wong E, Antonovsky N, Ludwig A, Sagi I, Saftig P, Tessier-Lavigne M, Yaron A (2014) ADAM metalloproteases promote a developmental switch in responsiveness to the axonal repellant Sema3A. Nat Commun 5:4058. Medline

Ruiz JM, Rodríguez J, Bovolenta P (2009) Growth and differentiation of the retina and the optic tectum in the medaka fish requires olSfrp5. Dev Neurobiol 69:617–632. CrossRef Medline

Sánchez-Camacho C, Bovolenta P (2008) Autonomous and non-autonomous Shh signalling mediate the in vivo growth and guidance of mouse retinal ganglion cell axons. Development 135:3531–3541. CrossRef Medline

Sánchez-Camacho C, Bovolenta P (2009) Emerging mechanisms in morphogen-mediated axon guidance. Bioessays 31:1013–1025. CrossRef Medline

Satoh W, Gotoh T, Tsunematsu Y, Aizawa S, Shimono A (2006) Sfrp1 and Sfrp2 regulate anteroposterior axis elongation and somite segmentation during mouse embryogenesis. Development 133:989–999. CrossRef Medline

Saxena S, Caroni P (2007) Mechanisms of axon degeneration: from development to disease. Prog Neurobiol 83:174–191. CrossRef Medline

Sebastián-Serrano A, Sandonìs A, Cardozo M, Rodríguez-Tornos FM, Bovolenta P, Nieto M (2012) Palphax6 expression in postmitotic neurons mediates the growth of axons in response to SFRP1. PLoS One 7:e31590. CrossRef Medline

Suh LH, Oster SF, Soehrman SS, Grenningloh G, Sretavan DW (2004) L1/Laminin modulation of growth cone response to EphB triggers growth pauses and regulates the microtubule destabilizing protein SCG10. J Neurosci 24:1976–1986. CrossRef Medline

Tamada A, Kumada T, Zhu Y, Matsumoto T, Hatanaka Y, Muguruma K, Chen Z, Tanabe Y, Torigoe M, Yamauchi K, Oyama H, Nishida K, Murakami F (2008) Crucial roles of Robo proteins in midline crossing of cerebellofugal axons and lack of their up-regulation after midline crossing. Neural Dev 3:29. Medline

Terry K, Magan H, Baranski M, Burrus LW (2000) Sfrp-1 and sfrp-2 are expressed in overlapping and distinct domains during chick development. Mech Dev 97:177–182. CrossRef Medline

Thompson H, Barker D, Camand O, Erskine L (2006a) Slits contribute to the guidance of retinal ganglion cell axons in the mammalian optic tract. Dev Biol 296:476–484. CrossRef Medline

Thompson H, Camand O, Barker D, Erskine L (2006b) Slit proteins regulate distinct aspects of retinal ganglion cell axon guidance within dorsal and ventral retina. J Neurosci 26:8082–8091. CrossRef Medline

Thompson H, Andrews W, Parnavelas JG, Erskine L (2009) Robo2 is required for Slit-mediated intraretinal axon guidance. Dev Biol 335:418–426. CrossRef Medline

Trimarchi JM, Stadler MB, Cepko CL (2008) Individual retinal progenitor cells display extensive heterogeneity of gene expression. PLoS One 3:e1588. CrossRef Medline

Wang LC, Rachel RA, Marcus RC, Mason CA (1996) Chemosuppression of retinal axon growth by the mouse optic chiasm. Neuron 17:849–862. CrossRef Medline

Webber CA, Hocking JC, Yong VW, Stange CL, McFarlane S (2002) Metalloproteases and guidance of retinal axons in the developing visual system. J Neurosci 22:8091–8100. Medline

Weber S, Saftig P (2012) Ectodomain shedding and ADAMs in development. Development 139:3693–3709. CrossRef Medline